

## **Title page:**

# **PINN-based short-term forecasting of fault slip evolution during the 2010 slow slip event in the Bungo Channel, Japan**

**Masayuki Kano<sup>1,2</sup>** (ORCID: 0000-0002-7288-4760), **and Rikuto Fukushima<sup>3</sup>** (ORCID: 0009-0007-0463-1458)

- Masayuki Kano, Disaster Prevention Research Institute, Kyoto University, Japan, kano.masayuki.4m@kyoto-u.ac.jp
- Rikuto Fukushima, Department of Geophysics, Stanford University, U.S., rfukushima@stanford.edu

**Corresponding author: Masayuki Kano, masayuki.kano.a3@tohoku.ac.jp**

## Abstract

Monitoring and forecasting fault slip evolution are fundamental for understanding earthquake cycles and assessing future seismic hazards. This study proposes a physics-based data assimilation framework that integrates geodetic observations with fault mechanics introducing spatial heterogeneity in frictional properties, with a particular focus on short-term fault slip forecasting. The proposed method employs physics-informed neural networks (PINNs) to calculate fault slip evolutions and to optimize the spatial distribution of frictional properties and is applied to the 2010 slow slip event beneath the Bungo Channel, southwest Japan, by changing the data period to be assimilated. When only the initial phase of slip acceleration is assimilated, a velocity-weakening frictional region is inferred beneath southwest Shikoku, corresponding to the initial nucleation are of the slow slip event. Our results demonstrate that the PINN-based data assimilation framework successfully forecasts slow transient slip even when only slip acceleration data are assimilated, whereas forecasts based on frictionally homogeneous models result in unstable fast slip. This difference can be interpreted as a consequence of introducing frictional heterogeneity, which allows both the characteristic size of the slipping region and the critical nucleation size to be variable, leading to stable slip evolution consistent with observations. When longer observation periods are assimilated, a velocity-strengthening region emerges around the slip-weakening patch, progressively restricting the direction of slip propagation. This velocity-strengthening region is interpreted as a mechanical constraint imposed by fault physics, linking the slip regions required to reproduce the observed geodetic time series. These results highlight the capability of PINN-based data assimilation incorporating geodetic observations and fault mechanics. The proposed framework provides a promising approach toward more realistic fault slip monitoring and short-term forecasting, and offers a foundation for future extensions incorporating uncertainty quantification and probabilistic forecasting.

## **Keywords**

Slow slip event, Physics-informed neural networks, Data assimilation, Global Navigation

Satellite System, Bungo Channel, Frictional parameter

# Main Text

## Introduction

A wide spectrum of fault slip phenomena, including coseismic fast slip, afterslip, slow slip events (SSEs), and steady plate motion, has been observed in plate subduction zones. Monitoring these diverse fault slip processes provides a comprehensive understanding of the entire earthquake cycle, from interseismic strain accumulation to coseismic rupture and postseismic relaxation. Among these phenomena, SSEs, which are the primary focus of this study, are characterized by slow, transient fault motions with durations ranging from days to years, in contrast to rapid coseismic slip (e.g., Obara and Kato 2016). Although SSEs do not generate strong ground motions, seismic and geodetic evidence suggests that SSEs can play an important role in earthquake preparation processes: SSEs have been inferred to precede megathrust earthquakes (e.g., Kato et al. 2012; Ruiz et al. 2014), implying that SSEs may modulate stress conditions on adjacent locked fault segments. Therefore, continuous monitoring and quantitative characterization of SSEs are expected to provide valuable information for evaluating future slip potential. However, observational evidence alone is generally insufficient to forecast the future evolution of ongoing SSEs. This limitation motivates the development of physics-based forecasting frameworks that can integrate observations with fault mechanics to infer and forecast SSE evolution.

This study particularly focuses on short-term forecasting of SSEs using a physics-based approach. Data assimilation (DA), which dynamically integrates observation data with numerical modeling governed by physical laws, provides a promising framework for such physics-based forecasting (e.g., Lewis et al. 2006; Fletcher 2022). DA techniques were originally developed in meteorology and have been widely implemented in operational weather and ocean forecasting systems. More recently, a wide variety of DA methods have been

proposed for fault slip monitoring problems, including Markov chain Monte Carlo (MCMC) method (Fukuda et al. 2009; Kano et al. 2024), ensemble Kalman filter (Hirahara and Nishikiori 2019; van Dinther et al. 2019; Diab-Montero et al. 2023), particle filter (Mitsui et al. 2010; Hori et al. 2014), adaptive Gaussian mixture filter (Diab-Montero et al. 2025), particle flow filter (Diab-Montero et al. 2025), and adjoint method (Kano et al. 2013; 2015; Ohtani et al. 2025). Most of these studies have primarily focused on developing DA methodologies to optimize fault slip properties, i.e., frictional parameters that control fault slip behavior. As a result, these approaches have largely been validated through numerical experiments rather than real observation data.

Kano et al. (2024, hereafter K24) were the first to apply DA to real SSE observations recorded during the 2010 Bungo Channel SSE in southwest Japan (Figure 1). In K24, the subducting plate interface was modeled as a planar rectangular fault consisting of a single circular SSE patch, originally adopted by Hirahara and Nishikiori (2019). K24 estimated spatially uniform frictional parameters within the SSE patch while fixing its geometry. Despite these strong constraints, they demonstrated that such a simplified fault model could reproduce the long-term trend of the observed SSE signal.

K24 further investigated the short-term forecasting capability of their simplified model during an ongoing SSE. They demonstrated that assimilating observations from the slip acceleration phase alone could lead to a forecast of fast slips without imposing any prior constraints on the frictional parameters to restrict the solution to SSEs. This behavior was interpreted as resulting from the critical nucleation size,  $R_c$ , calculated from the estimated frictional parameters being smaller than the fixed radius of the SSE patch,  $R$ , thereby leading to unstable slip (Chen and Lapusta 2009).

Subsequently, Fukushima et al. (2025) relaxed the strong geometric and frictional constraints imposed in K24 by allowing for spatially heterogeneous frictional properties on the

fault. Although estimating spatially variable frictional parameters requires solving a high-dimensional optimization problem, they showed that an emerging machine-learning approach — physics-informed neural networks (PINN; Raissi et al. 2019) — can successfully address this challenge. Through numerical experiments, Fukushima et al. (2025) showed that PINN can reconstruct a spatially heterogeneous SSE fault patch.

Building on this work, Fukushima et al. (2026) applied the PINN-based DA framework to the real SSE observations used in K24 and revealed an ellipsoidal SSE patch beneath the Bungo Channel, achieving a quantitatively improved fit to geodetic observations. To our knowledge, their fault slip model represents the first quantitative result that simultaneously explains observed surface deformation and satisfies the fault mechanics in terms of fault slip monitoring. As a next step, the present study extends their PINN-based DA approach to short-term forecasting of fault slip, and investigates how the introduction of frictional heterogeneity influences slip forecast performance.

## **PINN-based DA framework**

PINNs incorporate observation data into physics-based models using neural networks (NNs). This section summarizes the PINN-based DA framework adopted in this study, including the Global Navigation Satellite System (GNSS) observations and the Bungo Channel SSEs, the governing equations and fault model, and the problem settings of the PINN. To enable a direct comparison with the DA results of K24, we use the same GNSS data and fault model as those adopted in K24.

### *GNSS observations and the Bungo Channel SSEs*

Geodetic observations have revealed that SSEs with durations of approximately 1.0 yr and moment magnitude of  $\sim$ 6.8–6.9 repeatedly occurred beneath the Bungo Channel in southwest Japan, where the Philippine Sea Plate subducts beneath the Amurian Plate (Figure 1) (Hirose et al. 1999; Kobayashi and Yamamoto 2011; Ozawa et al. 2013; Yoshioka et al., 2015; Seshimo and Yoshioka 2022). Crustal deformation associated with these SSEs has been continuously observed by the GNSS Earth Observation Network System (GEONET), operated by the Geospatial Information Authority of Japan. We used GNSS data from 86 GEONET stations (Figure 1), consistent with K24. The data were preprocessed using the GipsyX-1.4 software (Bertiger et al. 2020) to obtain daily position time series. This dataset is largely identical to that used in K24 (see K24 for details of the preprocessing procedure), except that we extend data period from 2006.5 to 2012.5, which is one year longer than in K24 and consistent with Fukushima et al. (2026). Linear trends during the inter-SSE period were estimated from the first two years (2006.5–2008.5) and removed from the entire time series. Figure 1b shows an example of the GNSS displacement time series at station 1059, which is located near the SSE source region. The SSE initiated around 2010 beneath southwest Shikoku and subsequently propagated westwards, lasting until approximately 2011 (Yoshioka et al. 2015; Fukushima et al. 2026). In the following analysis, we assimilate GNSS data using six different data periods starting from 2006.5 and ending at 2012.5, 2011.5, 2011.0, 2010.5, 2010.0, and 2009.5, respectively. The DA result using the full data from 2006.5 to 2012.5 corresponds to the case presented in Fukushima et al. (2026).

#### *Physics-based model of the Bungo Channel SSEs*

To calculate spatio-temporal evolution of SSEs, we adopt the fault model in the Bungo Channel originally introduced by Hirahara and Nishikiori (2019) and subsequently used in several studies (Kano et al. 2024; Ohtani et al. 2025; Fukushima et al. 2025; 2026). In this

model, the subducting plate interface is represented as a single planar rectangle fault with a dip angle of  $15^\circ$  and dimensions of  $120 \text{ km} \times 100 \text{ km}$  in the strike and dip directions, respectively. The center of the fault plane is located at a depth of 25 km. The entire fault is then subdivided into  $2 \text{ km} \times 2 \text{ km}$  subfaults, resulting in a total number of 3,000 subfaults is 3,000. In each subfault, fault slip evolution is assumed to obey the following governing equations:

$$\tau_i(t) = \sum_j k_{ij} (v_{\text{pl}} t - s_j(t)) - \frac{G}{2\beta} v_i(t), \quad (1)$$

$$\tau_i(t) = \tau_{0i} + a_i \sigma \ln\left(\frac{v_i(t)}{v_0}\right) + b_i \sigma \ln\left(\frac{v_0 \theta_i(t)}{L_i}\right), \quad (2)$$

$$\frac{d\theta_i(t)}{dt} = 1 - \frac{v_i(t)\theta_i(t)}{L_i}. \quad (3)$$

Equation (1) represents the quasi-dynamic equation of motion with radiation dumping (Rice 1993), while Equation (2) describes the rate- and state- dependent friction law with the aging law for state evolution given by Equation (3) (Dieterich 1979; Ruina 1983). In these equations,  $\tau_i(t)$ ,  $v_i(t)$ ,  $s_i(t)$  ( $= dv_i(t)/dt$ ), and  $\theta_i(t)$ , denote the shear stress, slip velocity, slip, and state variables at time  $t$ , are the simulation variables on subfault  $i$ , respectively. The slip response function  $k_{ij}$  represents the shear stress change on subfault  $i$  due to a unit slip on subfault  $j$  and is calculated assuming an isotropic, homogeneous elastic half-space (Okada 1992). The slip direction is assumed to be parallel to the relative plate motion of the subducting Philippine Sea plate to the Amurian plate (Sella et al. 2002). The plate velocity  $v_{\text{pl}}$ , shear modulus  $G$ , and shear wave velocity  $\beta$  are set to be 6.5 cm/yr (Miyazaki and Heki 2001), 40 GPa, and 3.0 km/s, respectively. The frictional parameters  $a_i$ ,  $b_i$ , and  $L_i$  control the fault slip behavior on each subfault. Slip stability is governed by the characteristic fault patch size  $R$  and the critical nucleation size  $R_c$ , defined in the following relationship (Chen and Lapusta 2009):

$$R_c = \frac{\pi}{4} \frac{GbL}{\sigma(b-a)^2}. \quad (4)$$

When  $R > Rc$ , fault slip becomes unstable and can result in seismic slip, whereas  $R < Rc$  leads to more stable slip. For example, Hirahara and Nishikiori (2019) successfully reproduced SSEs by prescribing a circular SSE patch with a radius of  $R = 35$  km and appropriate frictional parameters corresponding to  $R/Rc \sim 0.47$ . The reference shear stress  $\tau_0$  in Equation (2) corresponds to the shear stress for steady-state sliding at a reference velocity  $v_0$ , and the effective normal stress  $\sigma$  is set to be 100 MPa in this study. By combining Equations (1)–(3), we obtain an ordinary differential equation governing the temporal evolution of slip velocities, which can be written in the following form:

$$\frac{dv_i(t)}{dt} = \frac{\sum_j k_{ij} (v_{pl} - v_j(t)) - \frac{b_i \sigma}{\theta_i(t)} \left( 1 - \frac{v_i(t) \theta_i(t)}{L_i} \right)}{\frac{a_i \sigma}{v_i} + \frac{G}{2\beta}}. \quad (5)$$

#### *Problem setting of PINN-based DA*

PINNs provide a framework for obtaining solutions to differential equations with a set of model parameters (Raissi et al. 2019). PINNs provides a flexible framework for solving both forward and inverse problems, and have more recently been applied to inverse problems in seismology by integrating physics-based equations with observation data (e.g., Waheed et al. 2021; Rasht-Behesht et al. 2022; Rucker and Erickson 2024). In the present study, we employ PINNs for fault slip forecasting and frictional parameter optimization, following the framework of Fukushima et al. (2026). Below, we briefly summarize the PINN-based DA framework (see Fukushima et al. 2026 for details).

First, we introduce two fully-connected NNs to represent simulation variables and the spatial distributions of frictional parameters. The first network, NN\_A, takes time  $t$  and the two-dimensional fault locations  $(x, y)$  as inputs and outputs the slip velocity  $v(t, x, y)$  and the state variable  $\theta(t, x, y)$  at the corresponding time and location. The second network, NN\_B,

takes the spatial location  $(x, y)$  as inputs and outputs the corresponding frictional parameters  $a$ - $b(x, y)$ ,  $a(x, y)$  and  $L(x, y)$ . We adopt the same network architectures as those in Fukushima et al. (2026).

We then define the loss function  $J$  as the sum of the model residuals  $J_{\text{ode}}$ , the data misfit term  $J_{\text{data}}$ , and loss for initial condition  $J_{\text{ini}}$ :

$$J = J_{\text{ode}} + w_{\text{data}} J_{\text{data}} + w_{\text{ini}} J_{\text{ini}}, \quad (6)$$

$$J_{\text{ode}} = \frac{t^{*2}}{N_{ct} N_{cxy}} \sum_{i=1}^{N_{ct}} \sum_{j=1}^{N_{cxy}} \left( \bar{r}_v(t_i, x_j, y_j)^2 + \bar{r}_\theta(t_i, x_j, y_j)^2 \right), \quad (7)$$

$$\bar{r}_v(t_i, x_j, y_j) = \frac{1}{v_{\text{NN}}} \left( \frac{dv_{\text{NN}}}{dt} - f(v_{\text{NN}}, \theta_{\text{NN}}) \right), \quad (8)$$

$$\bar{r}_\theta(t_i, x_j, y_j) = \frac{1}{\theta_{\text{NN}}} \left( \frac{d\theta_{\text{NN}}}{dt} - g(v_{\text{NN}}, \theta_{\text{NN}}) \right), \quad (9)$$

$$J_{\text{data}} = \frac{1}{N_{\text{data}} N_t} \sum_{i=1}^{N_t} \left( (\mathbf{Hs}_{\text{NN}}(t_i) - \mathbf{d}_i)^T \mathbf{R}^{-1} (\mathbf{Hs}_{\text{NN}}(t_i) - \mathbf{d}_i) \right), \quad (10)$$

$$J_{\text{ini}} = \frac{1}{N_{cxy}} \sum_{i=1}^{N_{cxy}} \left( \log \frac{v_{\text{NN}}(0, x_i, y_i) \theta_{\text{NN}}(0, x_i, y_i)}{L_{\text{prior}}} \right)^2 \quad (11)$$

The weighting parameters are set to be  $w_{\text{data}} = 10^{-3}$  and  $w_{\text{ini}} = 10^{-4}$  following Fukushima et al. (2026). Equations (8) and (9) represent the residuals of the ordinary differential equations corresponding to Equations (5) and (3), respectively. We denote the right-hand sides of Equations (5) and (3) by  $f(v, \theta)$  and  $g(v, \theta)$ , respectively, and  $v_{\text{NN}}$  and  $\theta_{\text{NN}}$  represent the outputs of NN\_A.  $N_{ct}$  and  $N_{cxy}$  denote the numbers of collocation points in time and space, respectively, at which the residuals are evaluated. The collocation points are uniformly distributed in both time and space, with  $N_{ct} = 219$  and  $N_{cxy} = 3,000$ . The term  $J_{\text{ode}}$  is non-dimensionalized using the characteristic time  $t^*$  defined as  $L_{\text{prior}} / v_{\text{pl}}$  (Segall 2010), where  $L_{\text{prior}}$  is set to be 4.0 cm

following Hirahara and Nishikiori (2019). Equation (10) represents the data misfit between the calculated and the observed displacements. Here,  $\mathbf{d}_i$  consists of the observed displacements at the  $i$ -th epoch  $t_i$  for all GNSS stations, with a total length of  $N_{\text{data}}$ , and  $N_t$  is the total number of epochs. The variable  $\mathbf{s}_{\text{NN}}$  represents the slip at all subfaults, numerically integrated from  $\mathbf{v}_{\text{NN}}$ , and  $\mathbf{H}$  is the observation matrix that projects fault slip onto surface displacements at each GNSS station, calculated assuming an isotropic, homogeneous elastic half-space (Okada 1992). The covariance matrix for observations  $\mathbf{R}$  is set to be identical to that adopted in K24. Equation (11) imposes a constraint that the fault stress state at the initial epoch is close to steady-state conditions, which represents a prior information for regularizing inversion.

The loss function (Equation (6)) is minimized using the L-BFGS method (Liu and Nocedal 1989) until convergence or until the maximum number of iterations (40,000) is reached. To facilitate NN parameter optimization, we initialize the NN parameters using a transfer learning approach following Fukushima et al. (2026), in which the networks are pretrained using synthetic data generated based on the K24 results. The optimized NN parameters obtained at the final iteration are then used to calculate the spatio-temporal evolution of fault slip velocities, the corresponding surface deformation, and the spatial distribution of frictional parameters. We confirm that, in the following results, the model residuals  $J_{\text{ode}}$  are well converged. This is demonstrated by calculating the displacement time series using the estimated frictional parameters by PINNs using a traditional numerical solver, which is comparable to PINNs output.

## Results and Discussion

To evaluate the short-term forecasting capability of the PINN-based DA framework, we compare the calculated surface displacements with GNSS observations under different DA

periods. Figure 1b shows the displacement time series calculated using PINNs together with the observed GNSS time series for each DA window. In each panel, the black vertical line indicates the end time of the assimilated data period; model results after this point therefore correspond to forecasts based on the PINN estimation results. Regardless of the length of the assimilated data, all PINN-based models quantitatively reproduce the observed displacement time series during the assimilation period and achieve a significantly better fit than the results obtained by K24. This improvement is expected because the present PINN model incorporates spatially heterogeneous frictional properties, whereas K24 assumed spatially uniform friction (Fukushima et al. 2026). In contrast, the forecasted fault slip behavior differs substantially among the data periods. As demonstrated by K24, when DA is performed only up to the slip acceleration phase in a uniform friction model (e.g., data prior to 2010.5), the forecast tends to exhibit unstable fast slip unless prior constraints restricting the slip behavior to SSEs are imposed on the frictional parameters. In other words, it is essential to impose prior constraints to prohibit fast slip. In contrast, the PINN-based model forecasts slow transient slip even when only slip acceleration data are assimilated. This stabilization of fault slip behavior arises from the introduction of frictional heterogeneity, the physical implications of which are discussed below in terms of the estimated frictional parameters. In addition, the successful optimization of this high-dimensional inverse problem highlights the flexibility of NN representations, demonstrating that PINNs provide a powerful DA framework for fault slip monitoring and forecasting.

Figure 2 shows the estimated frictional parameters, with values on the order of  $10^{-3}$  for  $a-b$  and  $a$ , and on the order of centimeters for  $L$ . The inferred spatial patterns of these parameters vary depending on the length of the assimilated data period. When only data prior to the initiation of the SSE (i.e., before 2010.0) are assimilated, the PINN provides little

information on frictional parameters. This outcome is expected because the GNSS observations during this period do not contain clear transient deformations (Figure 3).

When data up to -2010.5 are assimilated, frictional heterogeneity with strong velocity weakening zone, i.e., large negative  $a-b$ , is clearly inferred beneath southwest Shikoku (Figure 3). In the model, SSE nucleation initiates in this region in early 2010 (Figure 4) to explain the observed large displacement in Shikoku (Figure 3), consistent with previous studies (Yoshioka et al. 2015; Fukushima et al. 2026). This nucleation behavior can be interpreted as a consequence of velocity-weakening frictional property and small  $L$  values in this region, which result in a small critical nucleation size  $R_c$  (Equation 4), and thus promote frictional instability (Fukushima et al. 2026). After its initiation, slip propagates to the surrounding regions (Figure 4). In K24, forecasts based on assimilation up to -2010.5 resulted in unstable fast slip. Fault slip stability is controlled by the ratio between the radius of the SSE patch  $R$  and critical nucleation size  $R_c$  (Chen and Lapusta 2009). In K24, only  $R_c$  could vary because the SSE patch geometry was fixed, whereas in the present study both  $R$  and  $R_c$  are allowed to vary through the introduction of frictional heterogeneity. As a result, the PINN-based forecasts exhibit stable slow slip behavior without imposing any prior constraints on the frictional parameters.

For longer assimilation periods (up to 2011.0, 2011.5, and 2012.5), the estimated frictional parameters and slip velocity distributions become largely consistent across models (Figures 2 and 4). In all cases, SSE nucleation occurs within the velocity-weakening patch beneath southwest Shikoku (Figure 3), followed by slip propagation into the surrounding regions. A notable difference among these models lies in the direction of slip propagation, which becomes increasingly restricted westward as the assimilated data period becomes longer. This behavior reflects the emergence of velocity-strengthening regions that progressively surround the velocity-weakening zone (Figures 2 and 4), thereby inhibiting slip propagation across these areas. To further examine this effect, we focus on the data misfit term  $J_{\text{data}}$

evaluated only over the period 2008.5–2010.5, during which the SSE initiates beneath southwest Shikoku and propagates westward.  $J_{\text{data}}$  takes almost the same values of  $\sim 1.53$  for both cases with assimilation periods of up to 2010.5 and 2011.5, respectively. This indicates that the ability to explain the observed GNSS time series is comparable between these two models and that we cannot distinguish whether the slip propagates in a circular way or only westwards from observation only during 2008.5–2010.5. By assimilating longer observation after 2010.5, we can infer the subsequent slip west of the Bungo Channel to explain large displacement in Kyushu (Figures 3 and 4). As a result, propagation of slip direction is restricted to keep the mechanical consistency between the initial and the subsequent slips, which leads to update the shape of the velocity-weakening region as well as the appearance of the surrounding velocity-strengthening regions. This results suggest that PINN-based inversion mitigate the non-uniqueness of the slip distributions by imposing fault mechanics as a regularization.

## Future Perspectives of fault slip monitoring and forecasting

We have demonstrated that the PINN-based DA approach substantially improves both the explanation of geodetic observations and the short-term forecasting of fault slip evolution compared to traditional DA methods such as K24. This improvement is primarily achieved by solving a large-dimensional optimization problem — namely, the estimation of spatially heterogeneous frictional parameters — by exploiting the flexible representation ability of NN. The general framework of PINN-based fault slip monitoring and forecasting has now been largely established, and it can therefore be applied to other SSEs observed worldwide. More directly, frictional parameter distributions could be estimated by assimilating other SSEs that have occurred in the Bungo Channel, enabling systematic comparisons of similarities and differences among SSEs within the same framework. Assimilation of a series of multiple SSEs

would be an important step toward examining whether a single model can consistently explain multiple SSE cycles. Such applications may provide a more realistic description of fault friction, including possible temporal variations of frictional properties accompanied with fluid migration, which can be naturally implemented within the current PINN framework.

Further improvement of the PINN-based DA framework is essential for more practical fault slip monitoring and forecasting. In the present study, we focus on point estimates and do not quantify its uncertainty. However, uncertainty estimates of frictional parameters are crucial for assessing their reliability and the temporal changes. Incorporating uncertainty quantification would further enable probabilistic short-term fault slip forecasting. Bayesian approaches, such as Bayesian PINNs (Yang et al. 2021), can incorporate uncertainty quantification into the PINN framework by treating NN parameters as probabilistic variables, and have already been applied to seismological problems (e.g., Agata et al. 2023). Introducing Bayesian formulations therefore represents a promising direction for advancing both fault physics understanding and practical fault slip forecasting.

Another important perspective concerns how strongly fault mechanics should be enforced in DA. Traditional DA methods developed for fault slip problems, such as adjoint method (Kano et al. 2015; 2020; Ohtani et al. 2025) and MCMC method (Fukuda et al. 2009; Kano et al. 2024), impose fault mechanics as hard constraints, such that the inferred fault slip evolution strictly satisfies the governing equations throughout the entire time period, except for numerical errors. In contrast, in the PINN-based DA framework (Fukushima et al. 2025; 2026), the governing equations are incorporated as weak constraints through loss functions for ordinary differential equations, and thus mechanical consistency is not always guaranteed over the full data period. This distinction may be reasonable given that fault mechanics are still not fully understood. Although the reliability of fault mechanics remains under debate, several future directions can be considered within the PINN-based DA framework. One approach is to

incorporate PINN-based estimation of frictional parameters (NN\_B in this study) into traditional DA methods. In this hybrid approach, fault mechanics would remain hard constraints, and fault slip evolution would be obtained by directly integrating the governing equations, while high-dimensional frictional parameter estimation would be achieved using NN. Another approach is to explore the possibility of unknown or unmodeled physics. While the specific form of such physics is currently unclear, observation data that cannot be fully explained by existing governing equations may contain information about missing physical processes (Fukushima et al. 2026), potentially leading to new physical insights — a key potential of PINN-based methods (Raissi et al. 2019; Chen et al. 2021). A first step in this direction would be to investigate, through numerical experiments, how PINNs behave when different fault physics, such as different evolution laws, are assumed.

In conclusion, we proposed a PINN-based DA framework to fault slip forecasting and applied it to the 2010 Bungo Channel SSE. By introducing frictional heterogeneity and solving a high-dimensional optimization problem using PINNs, we found that short-term forecasts yield to slow transient slip without imposing any prior constraint on fault friction, whereas traditional DA methods with uniform friction predict unstable fast slip. Through this application, we demonstrated the capability of PINNs for fault slip forecasting. The PINN-based DA framework thus represents a promising step toward physically consistent and data-adaptive fault slip monitoring and forecasting.

## Declarations

### **Ethics approval and consent to participate**

Not applicable.

### **Consent for publication**

Not applicable.

### **List of abbreviations**

SSE: slow slip events; DA: data assimilation; MCMC: Markov chain Monte Carlo; PINN: physics-informed neural network; GNSS: Global Navigation Satellite System; NN: neural networks; GEONET: GNSS earth observation network system

### **Availability of data and materials**

The original GNSS data from GEONET used in this study can be downloaded from [https://www.gsi.go.jp/ENGLISH/geonet\\_english.html](https://www.gsi.go.jp/ENGLISH/geonet_english.html) after registration (GSI 2025). Prof. Takuya Nishimura and Dr. Yusuke Tanaka kindly provided the preprocessed data (Tanaka and Nishimura 2024). The original PINN code can be downloaded from <https://zenodo.org/records/14977672> (Fukushima 2025)

### **Competing interests**

The authors declare that they have no competing interests.

### **Funding**

This study was supported by the MEXT Project for Seismology toward Research Innovation with Data of Earthquake (STAR-E) (Grant number JPJ010217), and JSPS KAKENHI (Grant numbers JP24H01019, JP24K02951, JP25K01084, JP25K01104).

### **Authors' contributions**

MK designed this study and conducted PINN-based DA. RF developed the PINN code. MK conducted the overall analysis and prepared the manuscript. All authors discussed the results and approved the final manuscript.

### **Acknowledgements**

We appreciate the reviewers for their valuable comments on improving the manuscript and the editor for handling the manuscript. Figures were generated using Generic Mapping Tools (Wessel et al. 2013).

### **Authors' information**

<sup>1</sup>Disaster Prevention Research Institute, Kyoto University, Gokasho, Uji, Kyoto 611-0011, Japan. <sup>2</sup>Japan Agency for Marine-Earth Science and Technology, 3173-25, Showa-cho, Kanazawa-ku, Yokohama, 236-0001, Japan. <sup>3</sup>Department of Geophysics, Stanford University, 397 Panama Mall, Stanford, CA, 94305, U.S.

### **References**

Agata R, Shiraishi K, Fujie G (2023) Bayesian seismic tomography based on velocity-space Stein variational gradient descent for physics-informed neural network. *IEEE Transactions on Geoscience and Remote Sensing* 61:1–17. <https://doi.org/10.1109/TGRS.2023.3295414>

Bertiger W, Bar-Sever Y, Dorsey A, Haines B, Harvey N, Hemberger D, Heflin M, Lu W, Miller M, Moore AW, Murphy D (2020) GipsyX/RTGx, a new tool set for space geodetic operations and research. *Ad Space Res* 66(3):469–489. <https://doi.org/10.1016/j.asr.2020.04.015>

Chen T, Lapusta N (2009) Scaling of small repeating earthquakes explained by interaction of seismic and aseismic slip in a rate and state fault model. *J Geophys Res Solid Earth* 114(B1):B01311. <https://doi.org/10.1029/2008JB005749>

Chen Z, Liu Y, Sun H (2021) Physics-informed learning of governing equations from scarce data. *Nature communications* 12(1):6136. <https://doi.org/10.1038/s41467-021-26434-1>

Diab-Montero HA, Li M, van Dithner Y, Vossepoel FC (2023) Estimating the occurrence of slow slip events and earthquakes with an ensemble Kalman filter. *Geophys J Int* 234(3):1701–1721. <https://doi.org/10.1093/gji/ggad154>

Diab-Montero HA, Stordal AS, van Leeuwen PJ, Vossepoel FC (2025) Ensemble Kalman, adaptive Gaussian mixture, and particle flow filters for optimized earthquake occurrence estimation. *Computers Geosciences* 196:105836. <https://doi.org/10.1016/j.cageo.2024.105836>

Dieterich JH (1979) Modeling of rock friction: 1. experimental results and constitutive equations. *J Geophys Res Solid Earth* 84(B5):2161–2168. <https://doi.org/10.1029/JB084iB05p02161>

Fletcher SJ (2022) Data assimilation for the geosciences: from theory to application. Elsevier. Fukuda J, Johnson KM, Larson KM, Miyazaki S (2009) Fault friction parameters inferred from the early stages of afterslip following the 2003 Tokachi-oki earthquake. *J Geophys Res Solid Earth* 114(B4):B04412. <https://doi.org/10.1029/2008JB006166>

Fukushima R (2025) PINN\_3DSSE: Frictional Parameter Estimation on Slow Slip Events. (Zenodo). <https://doi.org/10.5281/ZENODO.14977672>

Fukushima R, Kano M, Hirahara K, Ohtani M, Im K, Avouac JP (2025). Physics-informed deep learning for estimating the spatial distribution of frictional parameters in slow slip regions. *J Geophys Res: Solid Earth* 130(5). <https://doi.org/10.1029/2024JB030256>

Fukushima R, Kano M, Hirahara K, Ohtani M (2026). Physics-Informed Deep Learning Links Geodetic Data and Fault Friction. arXiv [Physics.Geo-Ph]. arXiv. <https://doi.org/10.48550/arXiv.2601.20136>

Geodetic Observation Center, Geospatial Information Authority of Japan (2025) GNSS data. [https://doi.org/10.57499/GSI\\_GNSS\\_2025\\_001](https://doi.org/10.57499/GSI_GNSS_2025_001)

Hirahara K, Nishikiori K (2019) Estimation of frictional properties and slip evolution on a long-term slow slip event fault with the ensemble Kalman filter: numerical experiments. *Geophys J Int* 219(3):2074–2096. <https://doi.org/10.1093/gji/ggz415>

Hirose H, Hirahara K, Kimata F, Fujii N, Miyazaki S (1999) A slow thrust slip event following the two 1996 Hyuganada earthquakes beneath the Bungo Channel, southwest Japan. *Geophys Res Lett* 26(21):3237–3240. <https://doi.org/10.1029/1999GL010999>

Hori T, Miyazaki S, Hyodo M, Nakata R, Kaneda Y (2014) Earthquake forecasting system based on sequential data assimilation of slip on the plate boundary. *Theor Appl Mech Japan* 62:179–189. <https://doi.org/10.11345/nctam.62.179>

Kano M, Miyazaki S, Ito K, Hirahara K (2013) An adjoint data assimilation method for optimizing frictional parameters on the afterslip area. *Earth Planets Space* 65:1575–1580. <https://doi.org/10.5047/eps.2013.08.002>

Kano M, Miyazaki S, Ishikawa Y, Hiyoshi Y, Ito K, Hirahara K (2015) Real data assimilation for optimization of frictional parameters and prediction of afterslip in the 2003 Tokachi-oki earthquake inferred from slip velocity by an adjoint method. *Geophys J Int* 203(1):646–663. <https://doi.org/10.1093/gji/ggv289>

Kano M, Miyazaki S, Ishikawa Y, Hirahara K (2020) Adjoint-based direct data assimilation of GNSS time series for optimizing frictional parameters and predicting postseismic deformation following the 2003 Tokachi-oki earthquake. *Earth Planets Space* 72(1):1–24. <https://doi.org/10.1186/s40623-020-01293-0>

Kano M, Tanaka Y, Sato D, Iinuma T, Hori T (2024) Data assimilation for fault slip monitoring and short-term prediction of spatio-temporal evolution of slow slip events: application to the 2010 long-term slow slip event in the Bungo Channel, Japan. *Earth Planets Space* 76(1): 57. <https://doi.org/10.1186/s40623-024-02004-9>

Kato A, Obara K, Igarashi T, Tsuruoka H, Nakagawa S, Hirata N (2012) Propagation of slow slip leading up to the 2011 Mw 9.0 Tohoku-Oki earthquake. *Science* 335(6069), 705–708. <https://doi.org/10.1126/science.1215141>

Kobayashi A, Yamamoto T (2011) Repetitive long-term slow slip events beneath the Bungo Channel, southwestern Japan, identified from leveling and sea level data from 1979 to 2008. *J Geophys Res Solid Earth* 116(B4):B04406. <https://doi.org/10.1029/2010JB007822>

Lewis JM, Lakshmivarahan S, Dhall S (2006) Dynamic data assimilation: a least squares approach. Cambridge University Press.

Mitsui N, Hori T, Miyazaki S, Nakamura K (2010) Constraining interplate frictional parameters by using limited terms of synthetic observation data for afterslip: a preliminary test of data assimilation. *Theor Appl Mech Japan* 58:113–120.

<https://doi.org/10.11345/nctam.58.113>

Miyazaki S, Heki K (2001) Crustal velocity field of southwest Japan. *J Geophys Res* 106(B3):4305–4326. <https://doi.org/10.1029/2000JB900312>

Obara K, Kato A (2016) Connecting slow earthquakes to huge earthquakes. *Science* 353(6296):253–257. <https://doi.org/10.1126/science.aaf1512>

Ohtani M, Kame N, Kano M (2025) Development of an adjoint-based data assimilation method toward predicting SSE evolution: two-step optimization of frictional parameters and initial strength on the fault. *Earth Planets Space* 77(1):86. <https://doi.org/10.1186/s40623-025-02222-9>

Okada Y (1992) Internal deformation due to shear and tensile faults in a half-space. *Bull Seismol Soc Am* 82:1018–1040. <https://doi.org/10.1785/BSSA0820021018>

Ozawa S, Yarai H, Imakiire T, Tobita M (2013) Spatial and temporal evolution of the long-term slow slip in the Bungo Channel, Japan. *Earth Planets Space* 65(2):67–73. <https://doi.org/10.5047/eps.2012.06.009>

Raissi M, Perdikaris P, Karniadakis GE (2019) Physics-informed neural networks: A deep learning framework for solving forward and inverse problems involving nonlinear partial differential equations. *J Computational physics* 378:686–707. <https://doi.org/10.1016/j.jcp.2018.10.045>

Rasht-Behesht M, Huber C, Shukla K, Karniadakis GE (2022) Physics-informed neural networks (PINNs) for wave propagation and full waveform inversions. *J Geophys Res: Solid Earth* 127. <https://doi.org/10.1029/2021JB023120>

Rice JR (1993) Spatio-temporal complexity of slip on a fault. *J Geophys Res: Solid Earth* 98(B6):9885–9907. <https://doi.org/10.1029/93JB00191>

Rucker C, Erickson BA (2024) Physics-informed deep learning of rate-and-state fault friction. *Computer Methods in Applied Mechanics and Engineering* 430:117211. <https://doi.org/10.1016/j.cma.2024.117211>

Ruina A (1983) Slip instability and state variable friction laws. *J Geophys Res* 88(B12):10,359–10,370. <https://doi.org/10.1029/JB088iB12p10359>

Ruiz S, Metois M, Fuenzalida A, Ruiz J, Leyton F, Grandin R, Vigny C, Madariaga R, Campos J (2014) Intense foreshocks and a slow slip event preceded the 2014 Iquique  $M_w$  8.1 earthquake. *Science* 345:1165–1169. <https://doi.org/10.1126/science.1256074>

Sella GF, Dixon TH, Mao A (2002) REVEL: A model for Recent plate velocities from space geodesy. *J Geophys Res* 107(B4). <https://doi.org/10.1029/2000JB000033>

Segall P (2010) *Earthquake and Volcano Deformation*. Princeton University Press.

<https://doi.org/10.1515/9781400833856>

Seshimo Y, Yoshioka S (2022) Spatiotemporal slip distributions associated with the 2018–2019 Bungo Channel long-term slow slip event inverted from GNSS data. *Sci Rep* 12(1):343. <https://doi.org/10.1038/s41598-021-03982-6>

Tanaka Y, Nishimura T (2024) Input GNSS time series data for Tanaka et al. (2024), *JGR Solid Earth*. Zenodo. <https://doi.org/10.5281/ZENODO.14242258>

van Dinther Y, Künsch HR, Fichtner A (2019) Ensemble data assimilation for earthquake sequences: probabilistic estimation and forecasting of fault stresses. *Geophys J Int* 217(3):1453–1478. <https://doi.org/10.1093/gji/ggz063>

Waheed UB, Alkhalifah T, Haghigiat E, Song C, Virieux J (2021) PINNtomo: Seismic tomography using physics-informed neural networks. arXiv preprint. <https://doi.org/10.48550/arXiv.2104.01588>

Wessel P, Smith WH, Scharroo R, Luis J, Wobbe F (2013) Generic mapping tools: improved version released. *Eos* 94(45):409–410. <https://doi.org/10.1002/2013EO450001>

Yang L, Meng X, Karniadakis GE (2021) B-PINNs: Bayesian physics-informed neural networks for forward and inverse PDE problems with noisy data. *J Computational Physics* 425:109913. <https://doi.org/10.1016/j.jcp.2020.109913>

Yoshioka S, Matsuoka Y, Ide S (2015) Spatiotemporal slip distributions of three long-term slow slip events beneath the Bungo Channel, southwest Japan, inferred from inversion analyses of GPS data. *Geophys J Int* 201(3):1437–1455. <https://doi.org/10.1093/gji/ggv022>

## Figure legends

**Figure 1.** (a) The left panel shows the study area in southwest Japan, where the Philippine Sea Plate (PH) is subducting beneath the Amurian Plate (AM) along the Nankai Trough. The right

panel shows the Bungo Channel region indicated by the black rectangle on the left panel. The red rectangle indicates the SSE fault region originally introduced by Hirahara and Nishikiori (2019) and adopted by following reference studies (Kano et al. 2024; Fukushima et al. 2026). Green triangles represent GEONET stations used in this study. (b) Surface displacement time series at station 1059 shown in (a). Green, blue, and red dots indicate the daily GNSS time series in the trench-parallel (X), trench-perpendicular (Y), and vertical (Z) directions, respectively, while the red line represents the corresponding PINN-based calculations. The orange line indicates the calculations by the estimation of Kano et al. (2024). The black horizontal dotted line in each panel indicates the assimilation period.

**Figure 2.** Spatial distribution of the estimated frictional parameters (a)  $a-b(x,y)$ , (b)  $a(x,y)$ , (c)  $L(x,y)$ , and (d) critical nucleation length  $R_c(x,y)$ .  $R_c(x,y)$  is calculated only in the velocity-weakening region. In each subpanel, the end time of assimilated data are shown.

**Figure 3.** Observed (black) and calculated (orange) surface displacements during the period from 2008.5 to the end of each data assimilation period. The corresponding spatial distributions of the estimated frictional parameter  $a-b(x,y)$  for each period are also shown.

**Figure 4.** Spatio-temporal evolution of fault slip velocity corresponding to the timing of the top of each subpanel originating from 2006.5 as 0.0 yr. In each panel, the end time of assimilated data are shown by the white characters.

## Figures

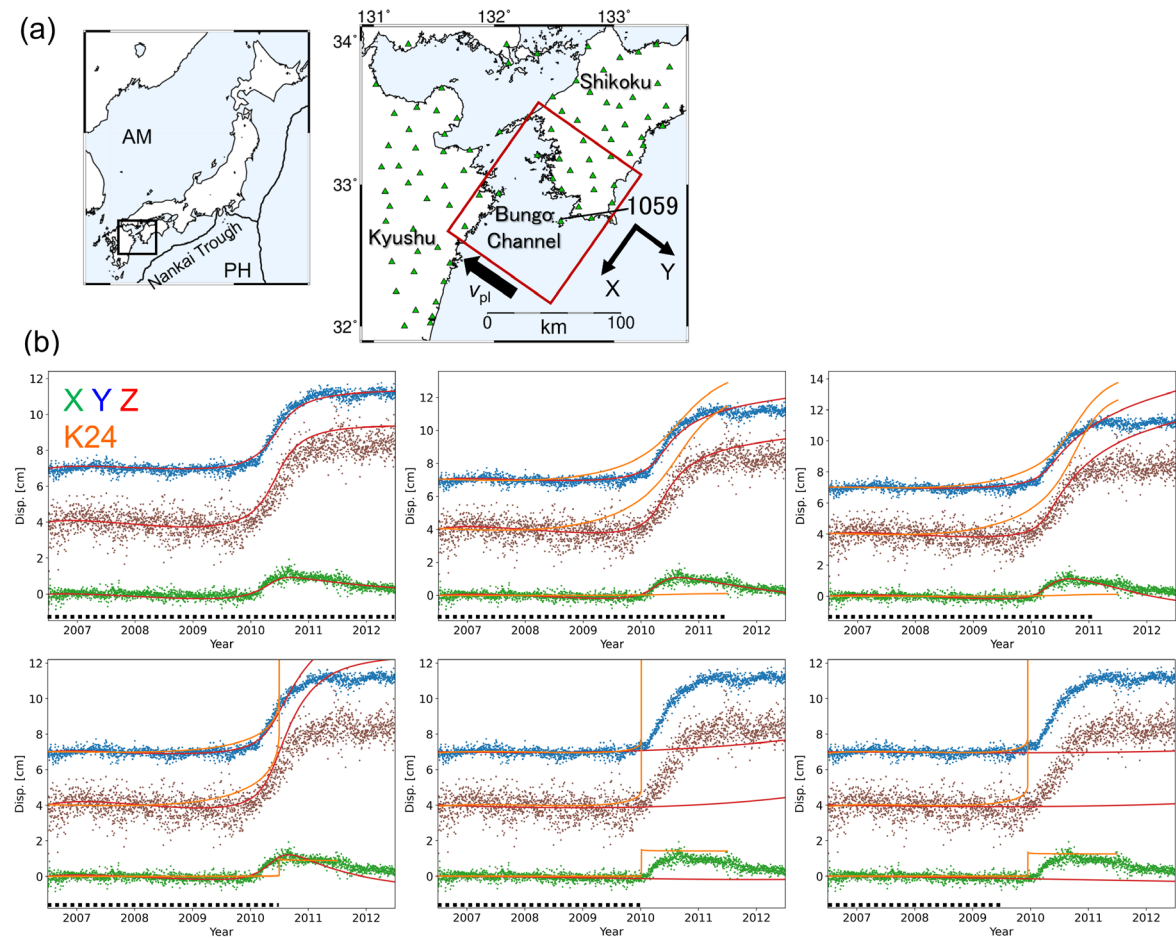


Figure 1

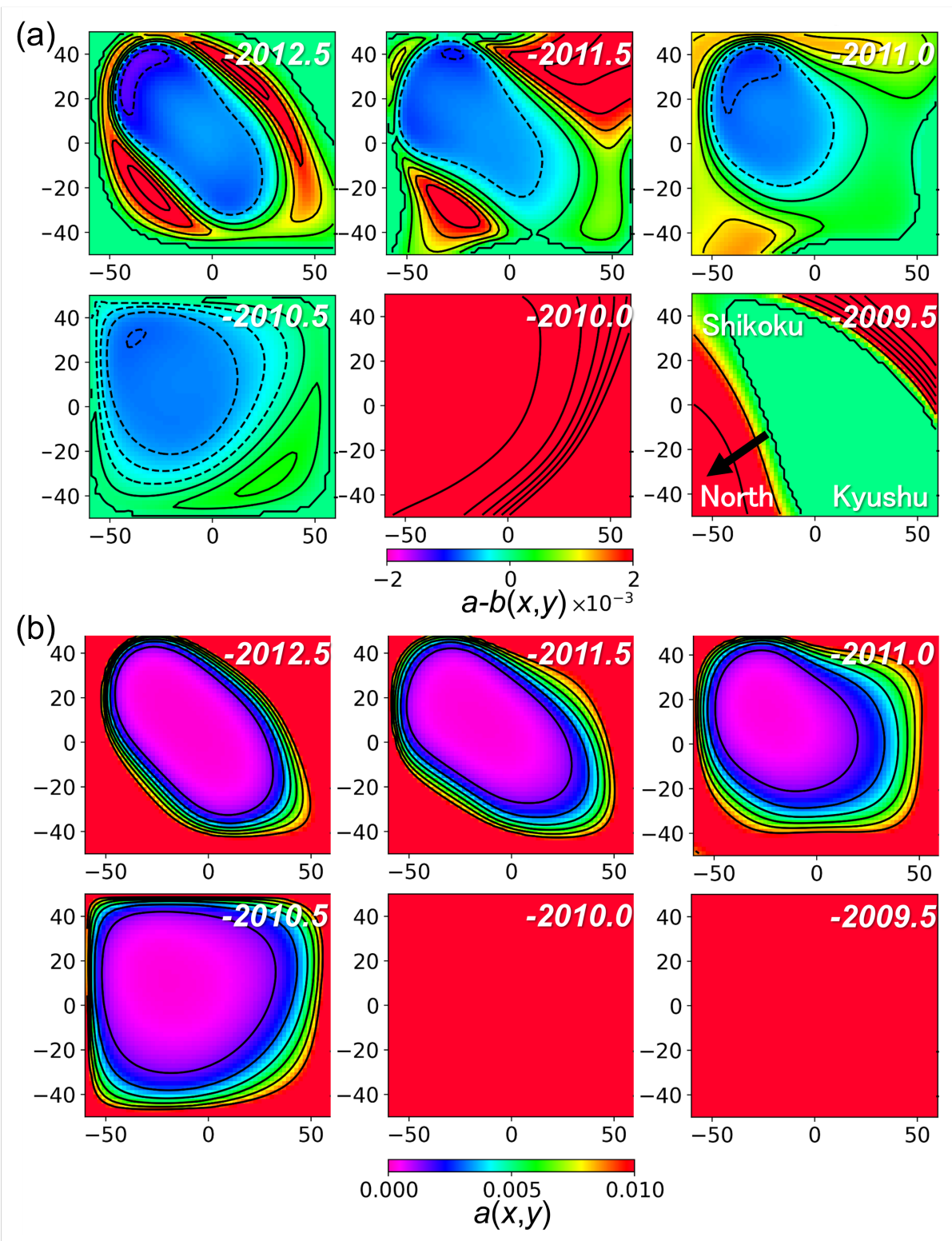


Figure 2

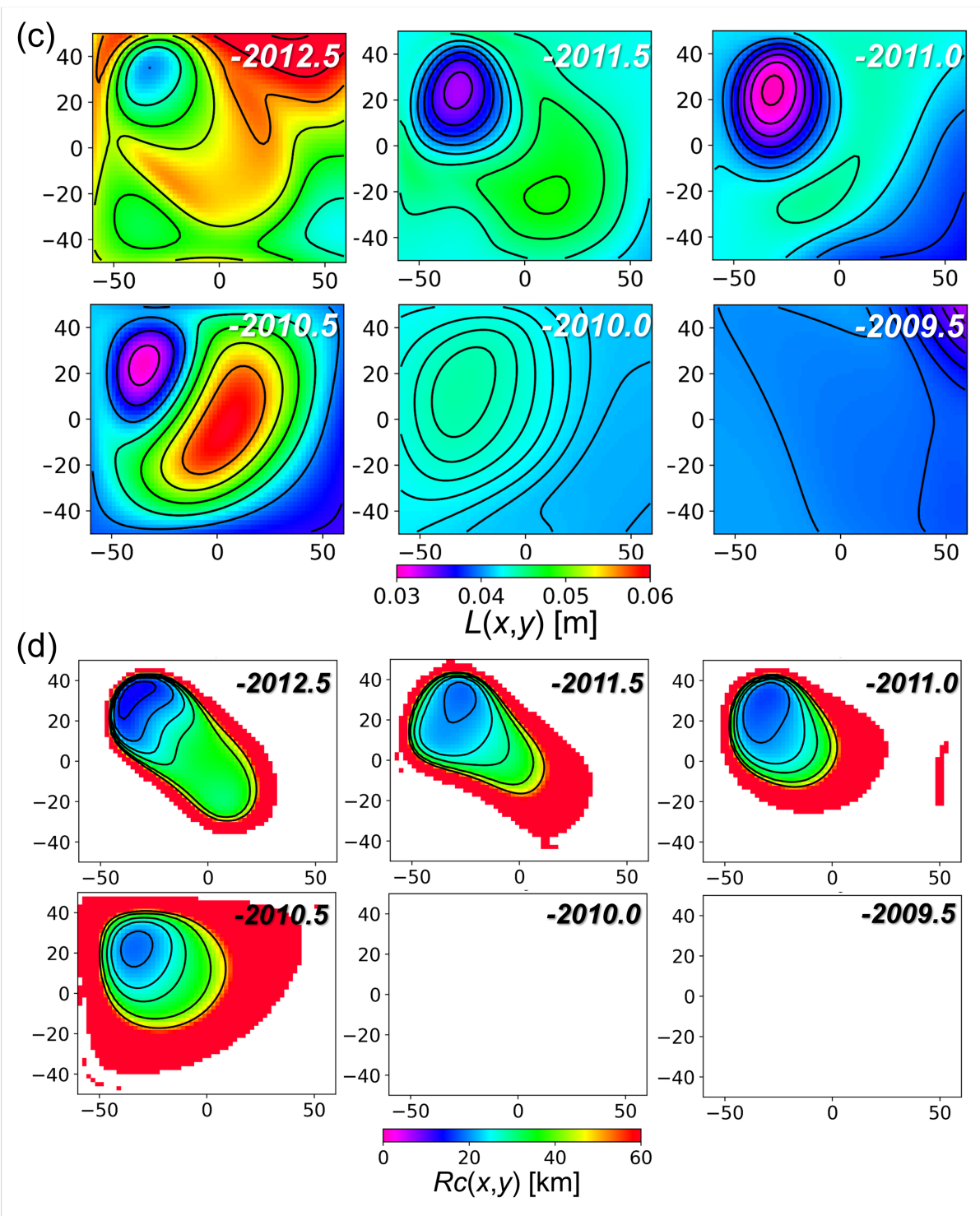


Figure 2 (continued)

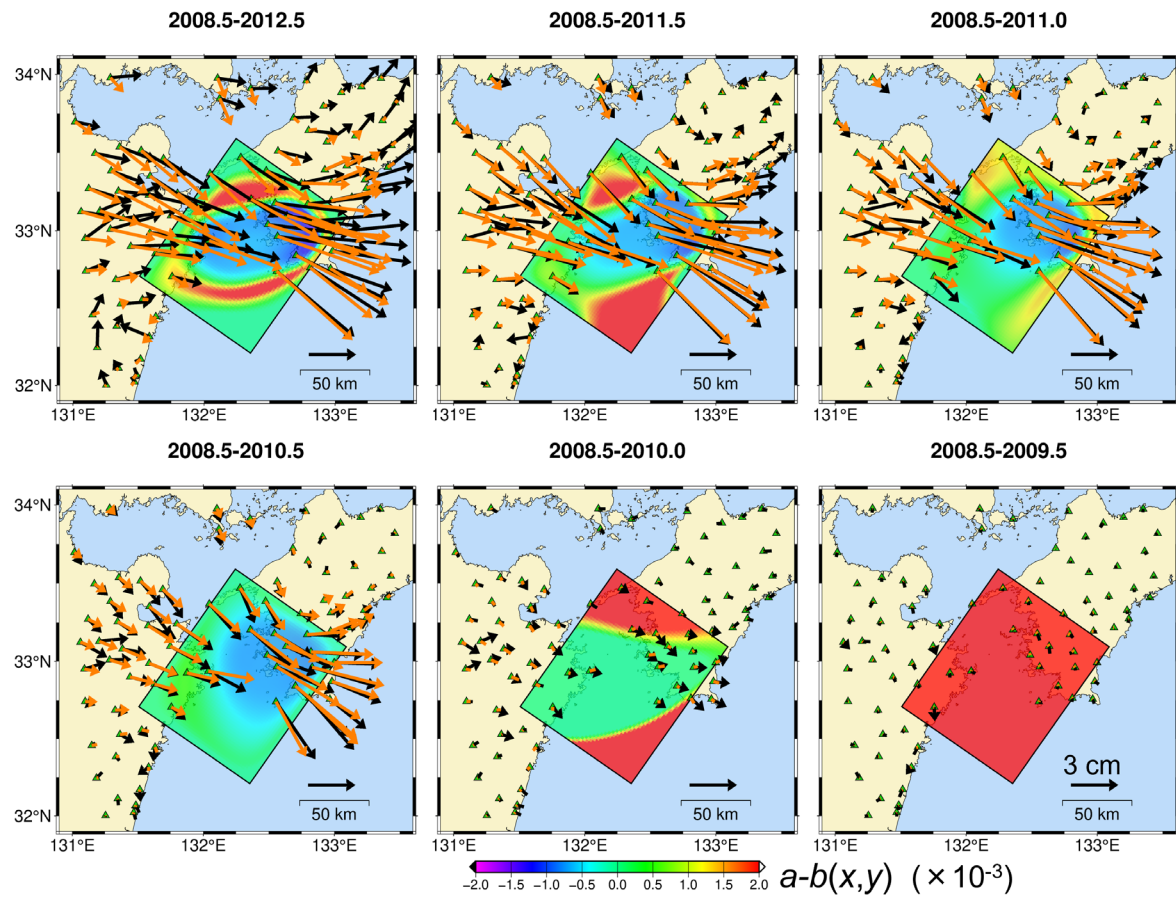


Figure 3

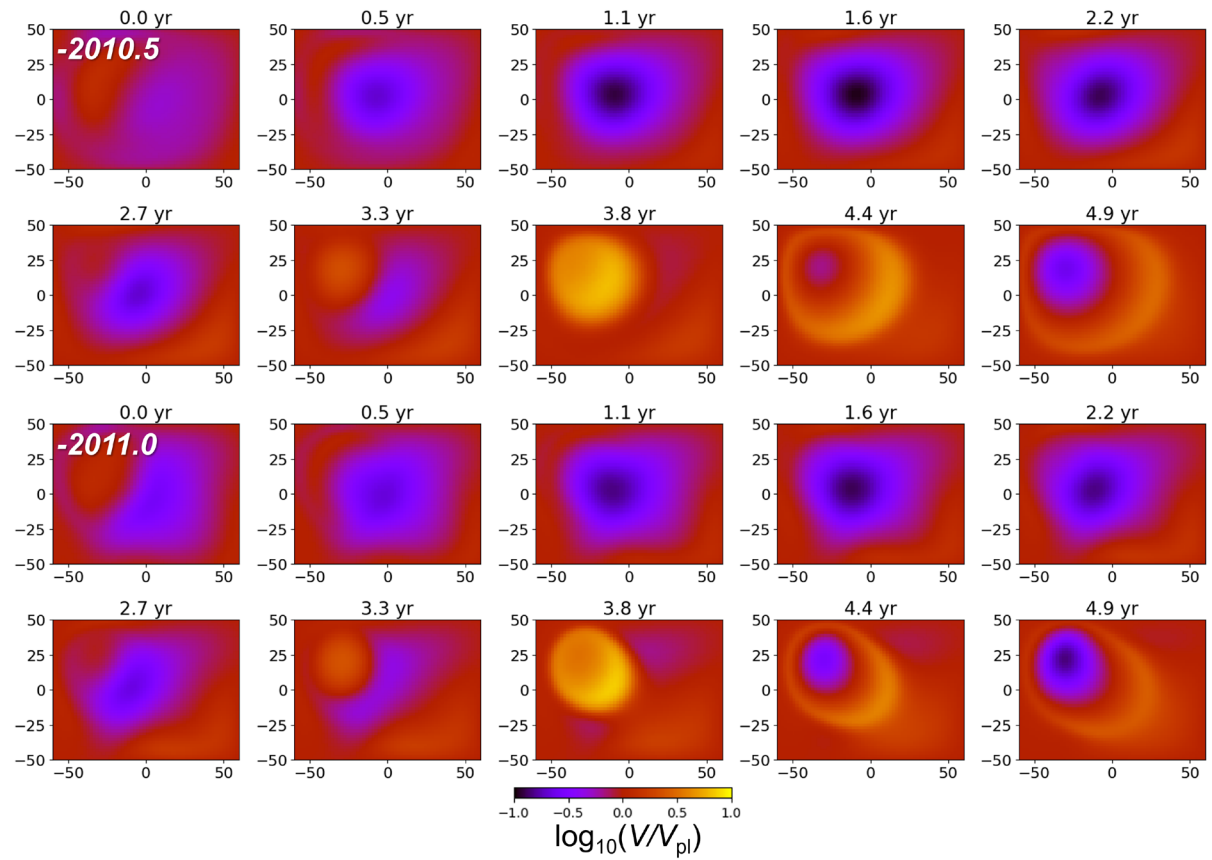
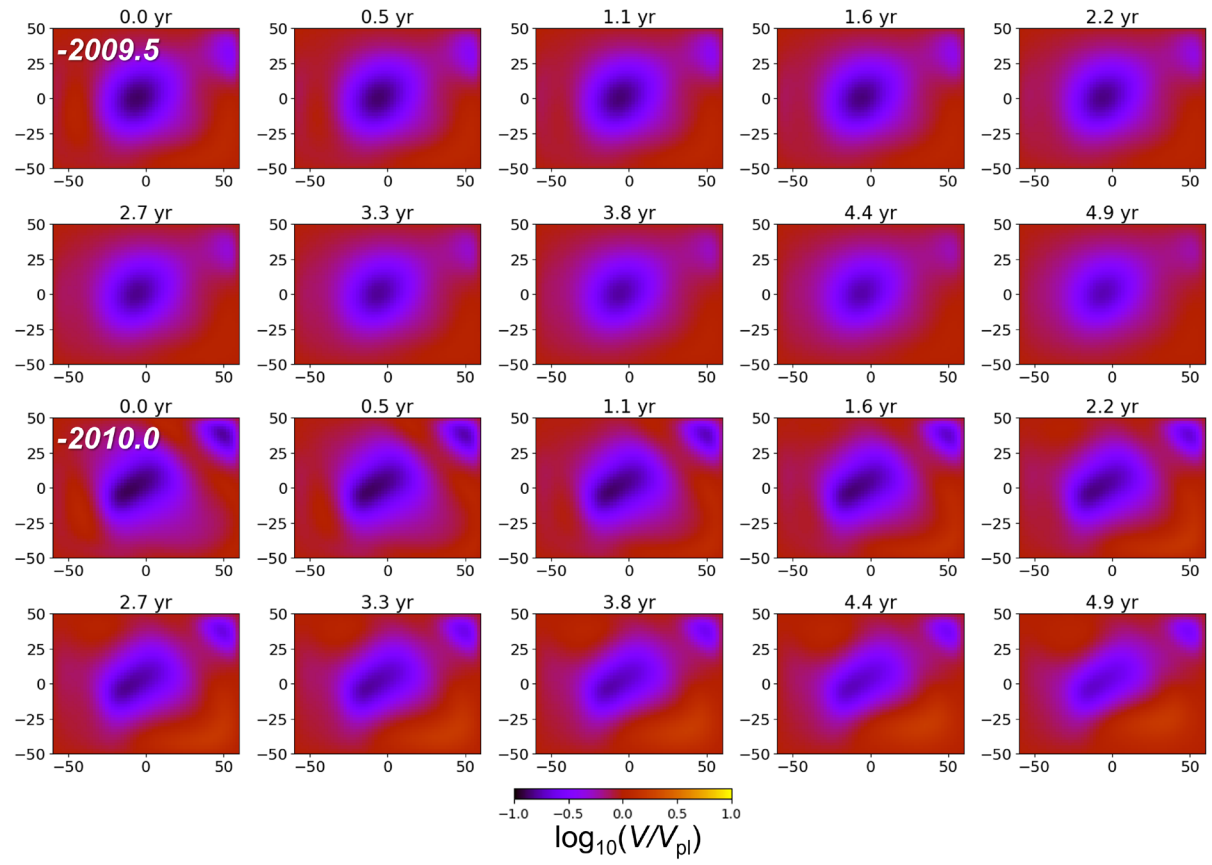


Figure 4

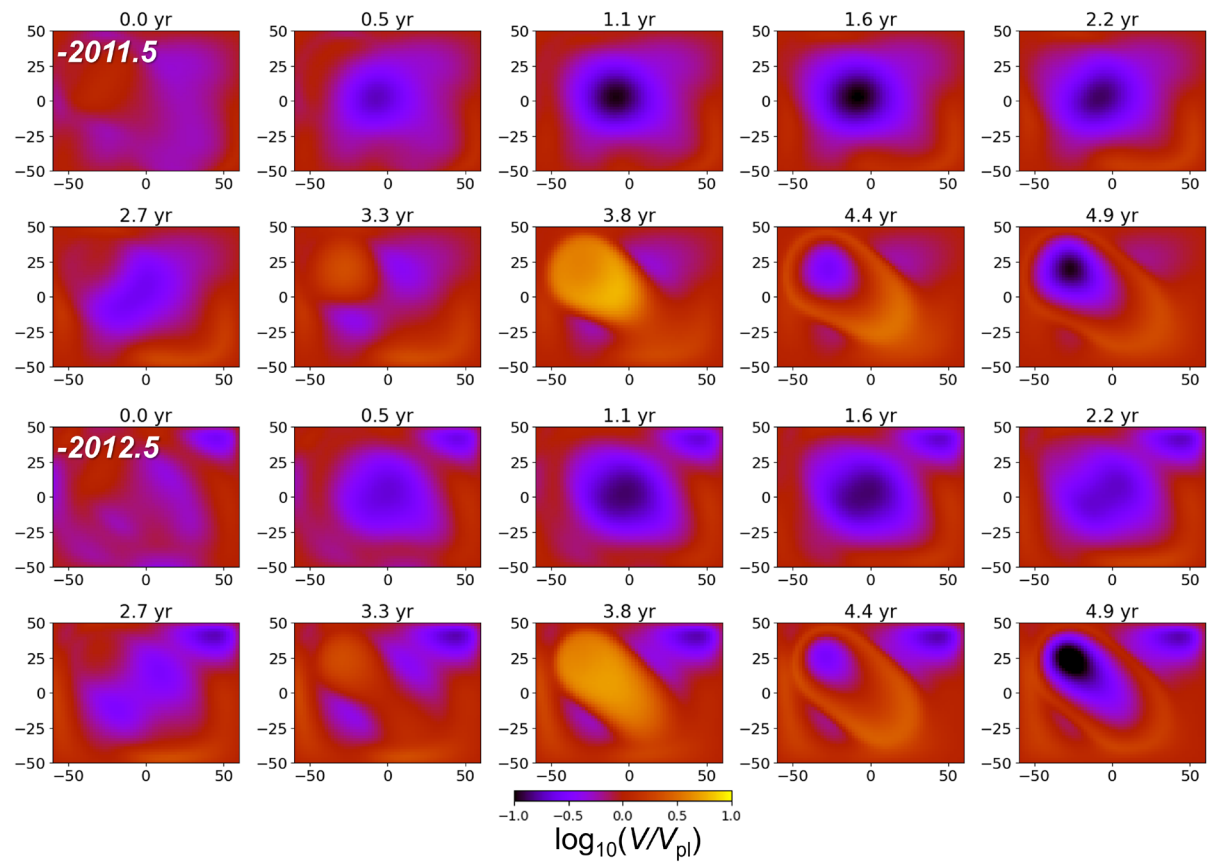


Figure 4 (continued)